Journal of Alloys and Compounds 521 (2012) 83–89

Contents lists available at SciVerse ScienceDirect

Journal of Alloys and Compounds

journal homepage: www.elsevier.com/locate/jallcom

Nanostructured hybrid cobalt oxide/copper electrodes of lithium-ion batteries with reversible high-rate capabilities

Yue Qi, Ning Du*, Hui Zhang, Jiazheng Wang, Yang Yang, Deren Yang

State Key Lab of Silicon Materials and Department of Materials Science and Engineering, Zhejiang University, Hangzhou 310027, People's Republic of China

ARTICLE INFO

Article history:
Received 29 October 2011
Received in revised form 5 January 2012
Accepted 7 January 2012
Available online 16 January 2012

Keywords:
Cobalt oxide
Cu nanorod arrays
Electrodeposition
Rf-sputtering
Anode
Lithium-ion batteries

ABSTRACT

We report the synthesis of nanostructured hybrid CoO/Cu electrodes through electrodeposition and sputtering. When applied as the anodes for lithium-ion batteries, the CoO/Cu nanowire arrays deliver long cycle life and enhanced power performance than CoO/Cu films. The large accessible surface area and improved electronic/ionic conductivity of the nanostructured electrodes may be responsible for the improved performance.

1. Introduction

Rechargeable lithium-ion batteries are currently the dominant power source for portable electronic devices due to their highest energy density among commercial rechargeable batteries, and considered to be the prime candidate for the next generation of electric vehicles [1]. However, the limited gravimetric capacity (372 mAh g^{-1}) of carbon has prompted intensive research for alternative anode materials that have good rate capability and enhanced cycling life [2]. Since the discovery of 3*d* transition-metal oxides could show good performance as the anode materials of Li-ion batteries, a great effort has been devoted to improve their capacity and cycling performance [3]. Among them, cobalt oxides (Co_3O_4, CoO) demonstrated the better electrochemical properties in lithium-ion batteries, than nickel oxide and iron oxides [4–6]. The reversible electrochemical reaction mechanism of the cobalt oxide was demonstrated as the formation and decomposition of Li_2O, accompanying the reduction and oxidation of Co nanoparticles (in the range of 1–5 nm), which is different from the classical Li insertion/deinsertion or Li-alloying processes [3]. However, cobalt oxide suffers from poor capacity retention due to the low electrical conductivity and large volume swings during the charge/discharge cycling [7–9]. Despite the improvements on the specific capacity and cyclability by using cobalt oxides nanomaterials [10–12], there are still great challenges in the preparation of nano-architectured CoO_x electrodes with high surface area, small crystal size and designed shapes.

Hybridizing nanostructured cobalt oxides with conducting matrices to form complex structures has been realized to be an effective route to overcome the above-mentioned problems [13–17]. More recently, Taberna et al. [18] demonstrated a two-step designed electrode consisting of Cu nanorods grown on a current collector followed by electrodeposition of Fe_3O_4 as an active material. This hybrid nanostructured electrode with large surface area and high electrical conductivity can shorten the lithium-ion diffusion path, which leads to high specific capacities and enhanced rate performance. Bi [19], Sn [20,21] and Ni_3Sn_4 [22] have also been deposited onto these nano-architectured Cu current collectors, which exhibited high-rate capability and long-cycle life.

Herein, we report the fabrication of nanostructured hybrid CoO/Cu electrodes through an electrodeposition and subsequent radio-frequency (RF)-sputtering approach. The nano-architectured current collector was obtained by growing a 3D array of Cu nanorods onto a Cu foil via electrodeposition assisted by a porous alumina membrane which was subsequently dissolved. The deposition of CoO onto Cu nanorods were achieved by controllable RF-sputtering, thus can form nanostructured hybrid CoO/Cu electrodes. When applied as the anode material for lithium-ion batteries, this nanostructured CoO/Cu electrode delivers high cycling life and enhanced power performance compared to planar electrodes.

* Corresponding author. Tel.: +86 571 87953190; fax: +86 571 87952322.
E-mail address: dna1122@zju.edu.cn (N. Du).

0925-8388/$ – see front matter © 2012 Elsevier B.V. All rights reserved.
doi:10.1016/j.jallcom.2012.01.046

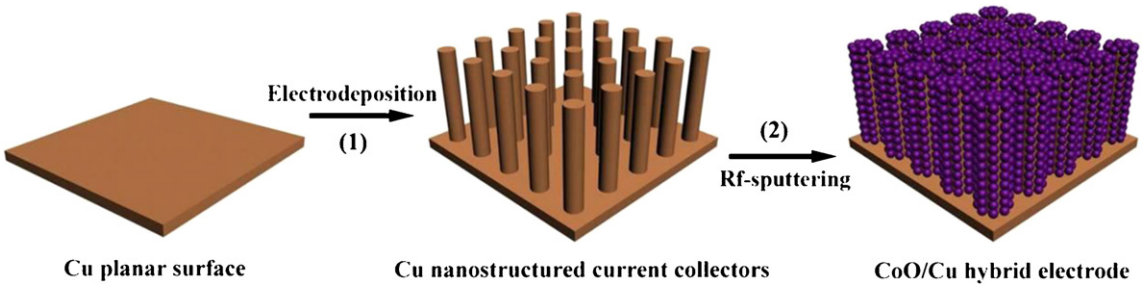

Fig. 1. Schematic of the fabrication of a nanostructured hybrid CoO/Cu electrode.

2. Experimental

All the chemicals were analytical grade without further purification. The fabrication process of nanostructured hybrid CoO/Cu electrodes is schematically shown in Fig. 1. It can be seen that the whole process involves in two steps: (1) fabrication of Cu nanorod arrays as current collectors, and (2) sputtering deposition of CoO onto the nanostructured current collectors. The two steps are detailedly described in the following sections.

2.1. Fabrication of Cu nanorod arrays

Arrays of highly perpendicular Cu nanorods on a copper disk substrate were fabricated by cathodic electrodeposition inside the nanopores of an alumina oxide membrane, with a LK2006A electrochemical work station. The deposition is proceeded on 1.5 cm diameter, 150-μm thick, 99.9% Cu foils within an electrolytic bath containing $CuSO_4{\cdot}5H_2O$ (Shanghai Chemical Reagent Co., Ltd.) 100 g L^{-1}, $(NH_4)_2SO_4$ (Huzhou Chemical Reagent Co., Ltd.) 20 g L^{-1} and diethyl-tri-amine (DETA, Sigma–Aldrich) 40 mL^{-1}. The AAO membrane (Whatman, Anodisc 47, reference 68095022) was 60-μm thick and the diameter of the membrane was 47 mm. The pore diameter was about 200 nm with a maximum porosity of about 50–65% and a pore density of 10^{10} cm^{-2}. Before electrodeposition, cathodes were mechanically polished with 1.0 μm alpha alumina and 0.25 μm gamma alumina polishing slurry, ultrasonically cleaned and rinsed with DI water. The polished Cu foil cathodes were further cleaned in ethanol and diluted HCl solution (10 vol%). The Cu foil anode, separator (filter paper soaked with electrolyte, Whatman), AAO template and polished Cu foil cathode were packed in sequence, and kept under a constant pressure by using several stainless-steel clamps. The outer parts of the cathode and anode were protected from dissolution or deposition by isolating the adhesive film.

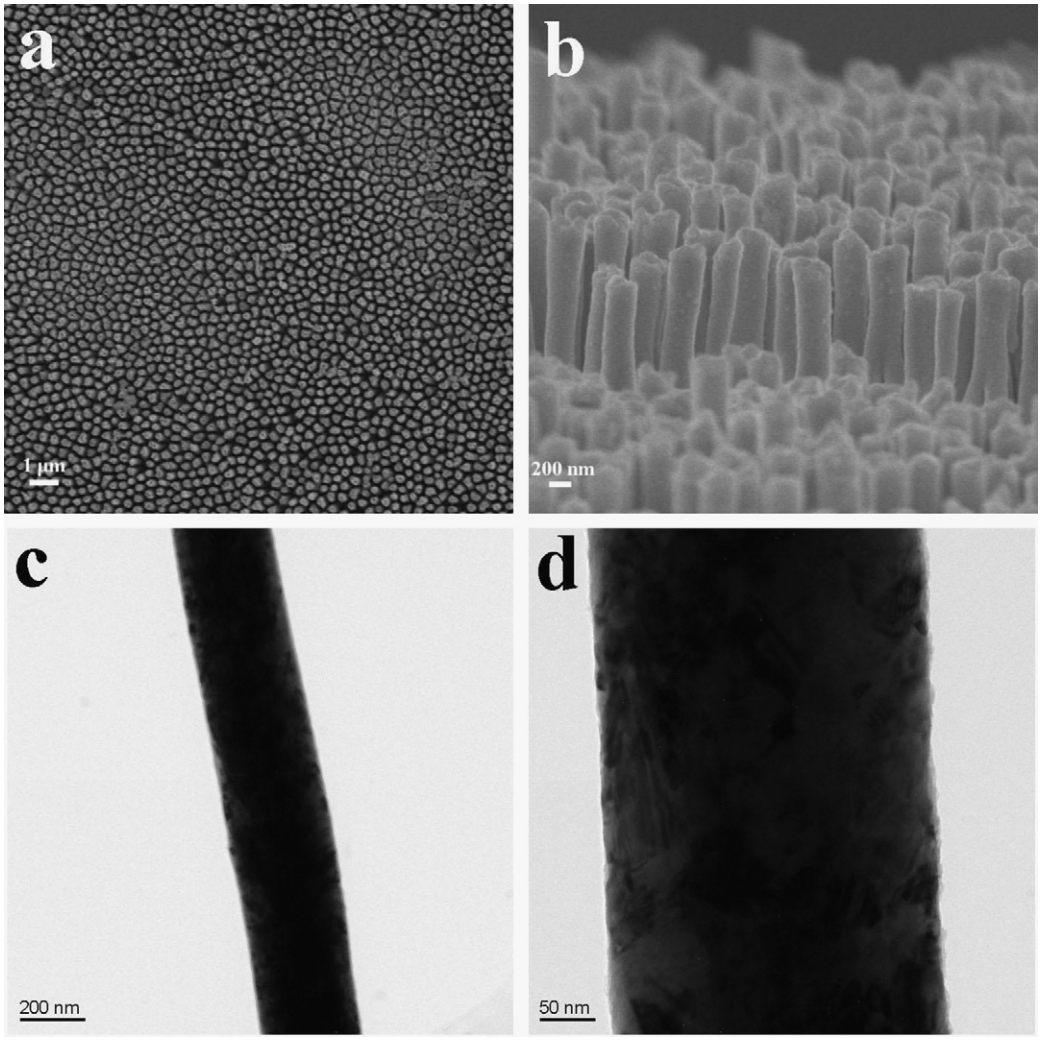

Fig. 2. Morphological and structural characterizations of Cu nanorod current collectors: (a) FESEM image of top view; (b) FESEM image of cross-sectional view; (c) TEM image; (d) magnified TEM image of single Cu nanorod.

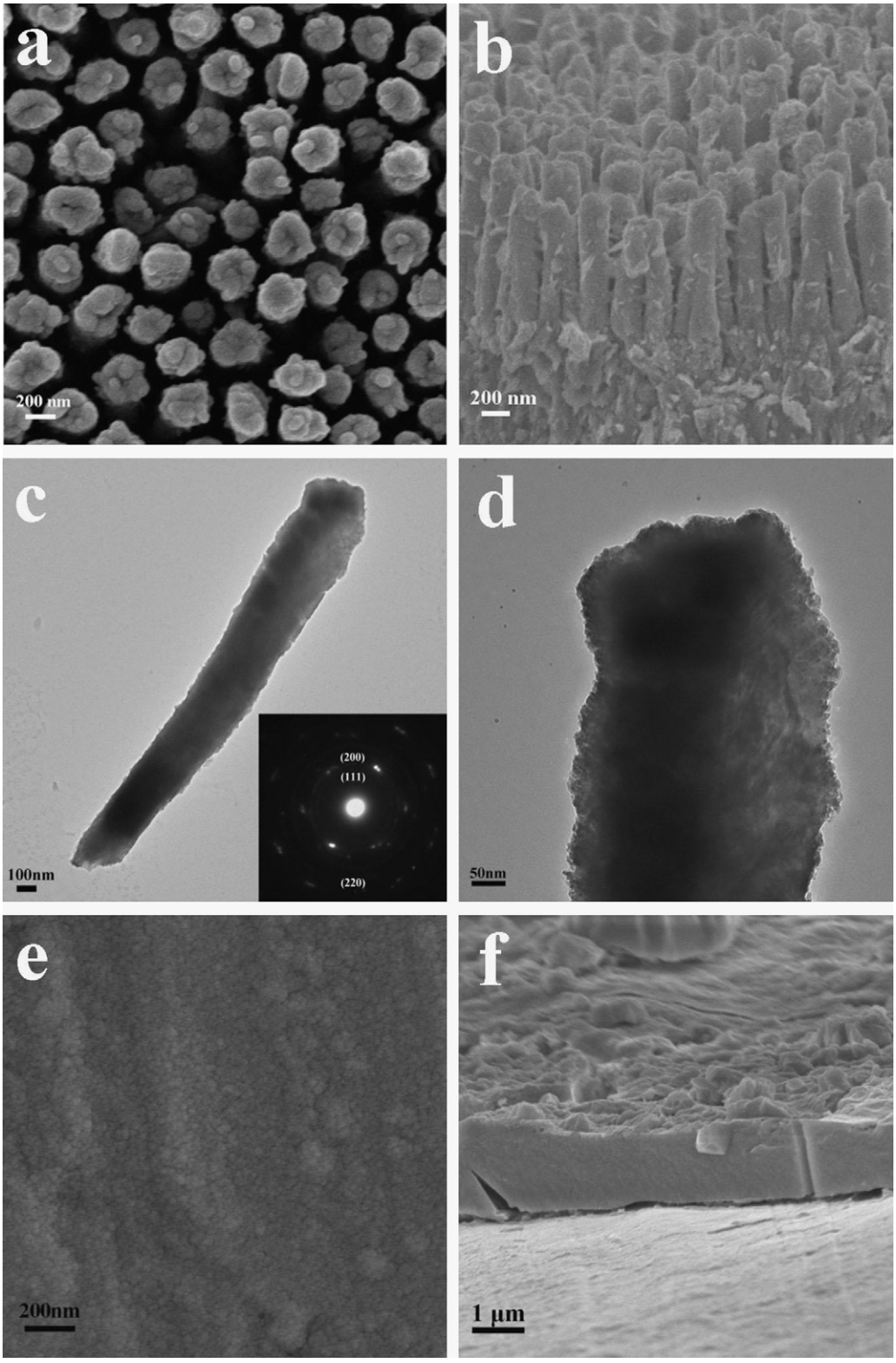

Fig. 3. Morphological and structural characterizations of nanostructured CoO/Cu electrodes: (a) FESEM image of top view; (b) FESEM image of cross-sectional view; (c) TEM image and its SAED pattern (inset); (d) magnified TEM image. FESEM images of planar CoO/Cu electrode: (a) top view and (b) cross-sectional view.

Electrochemical Cu deposit was achieved using a cyclic voltammetry technique by sweeping the potential from −0.8 V to −1.0 V at room temperature. After the electrodeposition, the cathodes were immersed in a 2 M NaOH solution for 30 min to remove the AAO templates and cleaned in the diluted HCl solution to remove the surface oxides.

2.2. Sputtering deposition of CoO

Cu nanorod arrays were covered with CoO layer by RF-sputtering deposition using a 99.99% CoO target at a working pressure of 10 Pa. The working gas for deposition was 99.99% pure argon and the gas flow was 20 sccm during sputtering. The

Cu substrate was deposited for 40 min at a sputtering power of 100 W and kept at 300 °C. After sputtering deposition, the load weight of CoO was measured to be 0.15 mg/cm^2.

2.3. Characterization

The obtained samples were characterized by X-ray powder diffraction (XRD) using a Rigaku D/max-ga X-ray diffractometer with graphite monochromatized Cu Kα radiation (γ = 1.54178 Å). The morphology and structure of the samples were examined by transmission electron microscopy (TEM, JEM-200 CX, 160 kV) and field emission scanning electron microscopy (FESEM, Hitachi S-4800) with energy-dispersive X-ray spectrometer (EDX).

2.4. Electrochemical measurements of CoO/Cu nanostructured electrodes

Electrochemical measurements were carried out using two-electrode cells with lithium metal as the counter and reference electrodes and the CoO/Cu nanostructured electrodes as the anodes. The electrolyte solution was 1 M $LiPF_6$ dissolved in a mixture of ethylene carbonate (EC), propylene carbonate (PC), and diethyl carbonate (DEC) with the volume ratio of EC/PC/DEC = 3:1:1. The cell assembly was performed in a glovebox filled with pure argon (99.999%) in the presence of an oxygen scavenger and a sodium drying agent. The electrode capacity was measured by a galvanostatic discharge–charge method at a current density of 215 mA g^{-1} (0.3 C) in the potential range of 0.01–2.5 V at 20 °C. Herein, 1 C is equal to 716 mA g^{-1}. Cyclic voltammetry (CV) were recorded on a MSTAT4 (Arbin Instruments) system in the potential range of 0.0–2.5 V at a scan rate of 0.1 mV s^{-1}. The electrochemical impedance spectroscopy (EIS) of the electrodes was performed on a CHI660D electrochemical workstation with an ac signal of 5 mV in amplitude and the frequency ranged from 0.01 Hz to 100 kHz. Before the EIS measurement, the electrodes were cycled for five cycles, then discharged to 2.0 V and kept until the open-circuit voltage stabilized.

3. Results and discussion

Cu nanorod arrays were electrodeposited on the surface of the mechanically polished Cu disks with assistance of an AAO template. Fig. 2a and b shows top and cross-sectional views of the Cu nanorod arrays on a current collector after removing the AAO membrane. The scanning electron microscopy (SEM) images clearly show the uniformly distributed Cu pillars with diameters of about 200 nm, as defined by the pore size of the AAO template. The Cu nanorods with smooth surface were perpendicular to the surface and the inter-rod distance was measured to be about 150 nm. The TEM images (Fig. 2c and d) of a single Cu nanorod further confirm the 1D structure of this current collector.

Deposition of CoO onto Cu nanorods was achieved by a RF-sputtering technique. Fig. 3 shows the SEM and TEM images of the nanostructured electrode after 40 min CoO deposition. The SEM images of top (Fig. 3a) and cross-sectional view (Fig. 3b) of the CoO/Cu electrode clearly demonstrate that the CoO has been uniformly deposited onto the surface of the Cu nanorods without any coalescence between them. The TEM images (Fig. 3c and d) of a single CoO/Cu hybrid nanorod indicate that the uniform CoO layer was continuous and the thickness of this layer was measured between 30 and 100 nm, which is consistent with the SEM pictures. According to the sputtering deposition technique and 1D array structure, the dispersion of CoO on the Cu nanorods was not homogeneous. It can be observed from Fig. 3c that more CoO was loaded on the top of the nanorod and the mass loading decreased along the nanorod. The polycrystalline structure of the CoO layer can be confirmed by its selected-area electron diffraction (SAED) pattern (Fig. 3c, inset). As observed, there are three diffraction rings corresponding to the (1 1 1), (2 0 0), and (2 2 0) planes of polycrystalline CoO, respectively. For comparison of the electrochemical performance with nanostructured CoO/Cu arrays, planar electrode was also prepared by direct sputtering CoO on Cu planar under the same conditions. The SEM images (Fig. 3e and f) confirm the formation of planar CoO/Cu electrode with uniform and smooth surface, and the thickness of the CoO layer was measured to be 150 μm from the cross-sectional view (Fig. 3f).

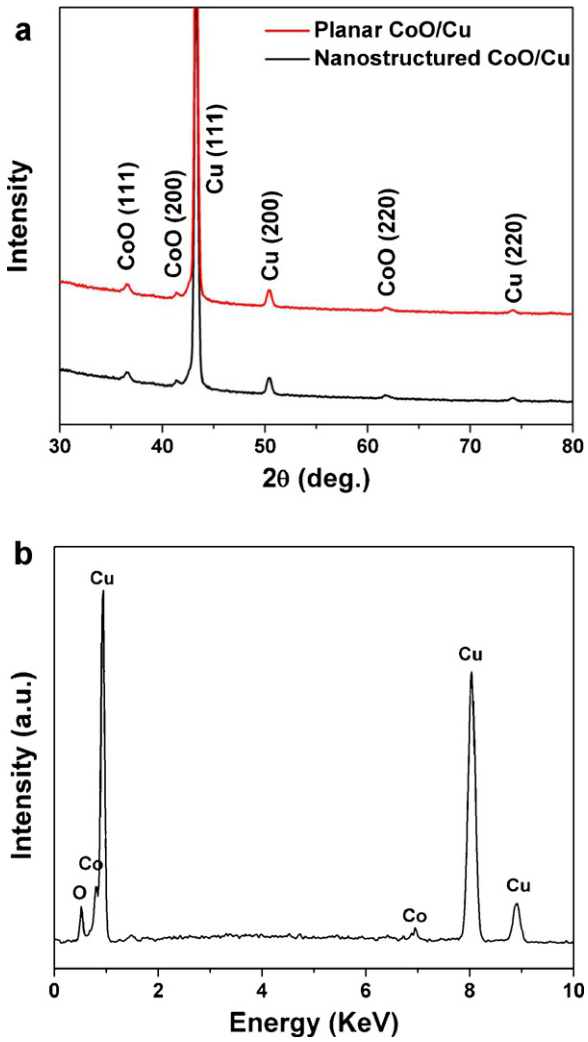

Fig. 4. (a) XRD patterns of the planar and nanostructured CoO/Cu electrodes; (b) EDX spectrum of the nanostructured CoO/Cu electrode.

Fig. 4a shows the XRD patterns of the as-prepared planar and nanostructured electrodes. There is little difference between these two patterns and all three peaks can be indexed to (1 1 1), (2 0 0), and (2 2 0) of cubic CoO phase (JCPDS: 43-1004), besides the reflections owing to metallic copper. This indicates the deposition of CoO layer onto the Cu substrates. Fig. 4b is the energy-dispersive X-ray (EDX) spectrum taken from the CoO/Cu hybrid nanorods. As observed, the strong peaks of Cu, Co, and O elements are expected from the Cu nanorods and the CoO layer, respectively. The above-mentioned characterizations confirm the successful synthesis of nanostructured CoO/Cu hybrid electrodes on a copper substrate.

Electrochemical tests were conducted by using the as-synthesized nanostructured electrodes as a potential anode and Li metal as a cathode. Fig. 5 shows the first three cyclic voltammogram (CV) curves of nanostructured CoO/Cu hybrid electrodes in the potential range of 0.0–2.5 V at a scan rate of 0.1 mV s^{-1}. The CV curves are in good agreement with the previous reported CoO anodes [23,24]. In the first cycle, a large cathodic current peak appears at 0.5 V which can be attributed to the formation of Li_2O and Co from the reduction of CoO. The cathodic peak at 0.5–0.8 V is also partly related to the formation of the SEI film. It is noticed that the cathodic peak at 0.5 V shifts to a higher potential, and become two peaks (one at 0.8 V and the other at 1.4 V) in the 2nd and 3rd cycles due to the pulverization of the CoO nanoparticles. During the

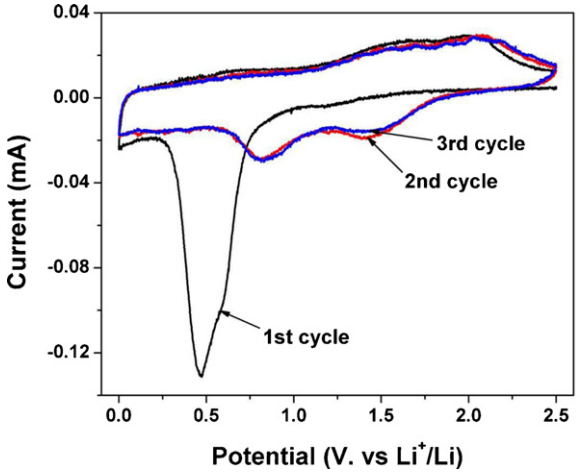

Fig. 5. First three CV curves of the nanostructured hybrid CoO/Cu electrode in the potential range of 0.0–2.5 V at a scan rate of 0.1 mV s^{-1}.

first lithiation process, the CoO particles are pulverized during Li-insertion and their surface energy is decreased due to interaction with the produced Li_2O, hence the potential of lithiation become higher in subsequent cycles. In the first anodic process, two oxidation peaks at 1.6 V and 2.0 V are attributed to the oxidation of CoO, and the anodic peaks changed slightly in the 2nd and 3rd cycles. Poizot et al. have reported that the electrochemical reaction mechanism of Li with transition metal oxides, such as CoO, mostly involves in a conversion reaction as follows [3],

$$CoO + 2Li \leftrightarrow Li_2O + Co$$

The electrochemical performance of as-synthesized nanostructured CoO/Cu hybrid electrodes was investigated and compared with the planar CoO/Cu electrodes. Fig. 6a and b displays the first three discharge–charge curves of the nanostructured CoO/Cu electrodes and planar CoO/Cu electrodes at a current density of 215 mA g^{-1} (0.3 C) and room temperature. As shown in Fig. 6a, the first discharge curve of the CoO/Cu electrodes has an extended potential plateaus at about 1.0 V, followed by a sloping potentials at about 0.5 V. The nanostructured electrodes delivers the first discharge capacity of 1362 mAh g^{-1} and the first charge capacity of 903 mAh g^{-1}, which indicates that its Coulombic efficiency is 66.3%. In contrast, the planar CoO/Cu electrode delivers initial discharge and charge capacities of 1416 mAh g^{-1} and 772 mAh g^{-1}, respectively, indicating that it has an initial Coulombic efficiency of 54.5%, which is much lower than that of the nanostructured electrode. The irreversible capacity loss of the CoO/Cu electrodes is mainly due to the formation of the solid-electrolyte interphase (SEI) layer and partial irreversible electrochemical reactions during further cycling because of the Co aggregation [25]. Compared to the planar electrode, the nanostructured CoO/Cu electrode could improve

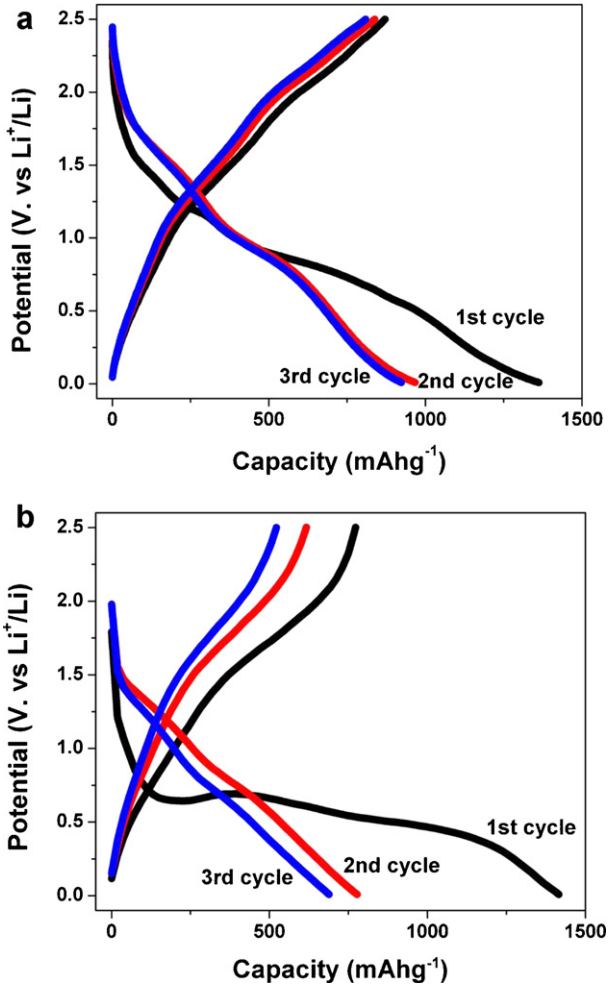

Fig. 6. First three discharge–charge curves of the nanostructured CoO/Cu electrode (a) and planar CoO/Cu electrode (b) based anode material at a current density of 215 mA g^{-1} (0.3 C) at room temperature.

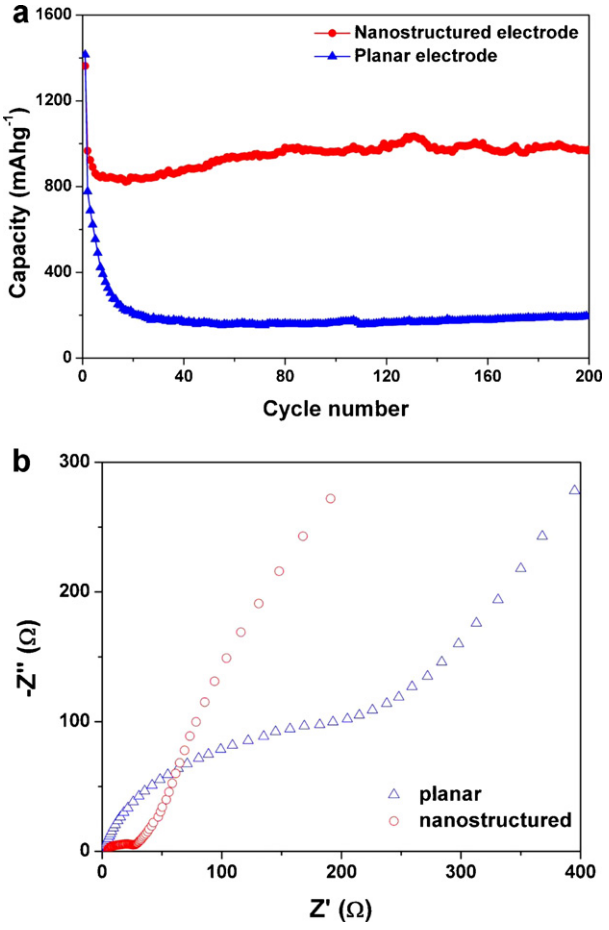

Fig. 7. (a) Discharge capacity versus cycle number for the nanostructured CoO/Cu electrode and planar electrode at a current density of 215 mA g^{-1} (0.3 C) at room temperature. Here, 1 C is equal to 716 mA g^{-1}. (b) Nyquist plots of nanostructured CoO/Cu electrode and planar electrode obtained by applying a sine wave with amplitude of 5 mV over the frequency range 100 kHz to 0.01 Hz.

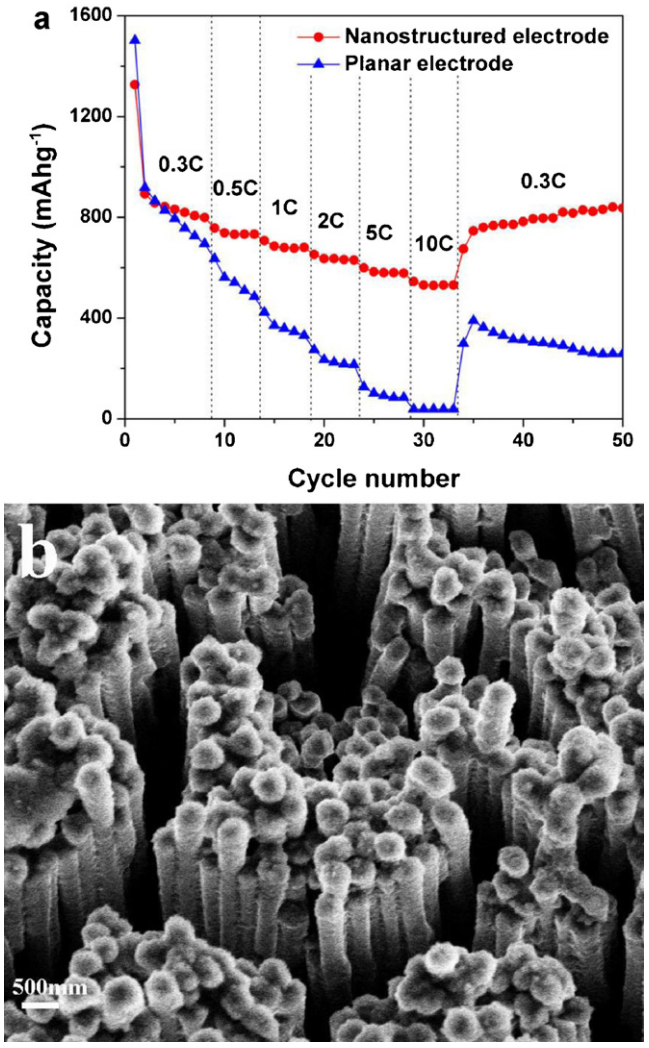

Fig. 8. (a) Specific capacities of the nanostructured CoO/Cu electrode and planar electrode for different discharge/charge cycles at various C rates. Here, 1 C is equal to 716 mA g^{-1}. (b) SEM image of the nanostructured electrode after the cycling test.

the electronic/ionic conductivity of the CoO/Co^0/Li_2O matrix and prevent Co particles from aggregating somehow, resulting in an improved initial Coulombic efficiency.

Fig. 7a shows the discharge capacity versus cycle number for the nanostructured hybrid CoO/Cu electrode and planar CoO/Cu electrode at a current density of 215 mA g^{-1} (0.3 C) at room temperature. It can be seen that the capacity of nanostructured CoO/Cu electrode experiences a gradual increasing process and stabilizes at 970 mAh g^{-1} after 200 discharge/charge cycles. Similar capacity rising phenomena have been observed from transition-metal oxides composite anode materials [26–28]. The reversible formation of polymeric gel-like film, which results from the decomposition of electrolyte, can be responsible for the capacity rising phenomena [29,30]. In contrast, the capacity behavior of the planar electrode shows a sharp and constant decrease associated with huge volume change and aggregation of the Co particles during the electrochemical process.

EIS was used to understand the relevance of morphology and surface area of the nanostructured CoO/Cu electrode and the planar electrode with the electrochemical performance in terms of the total internal electrochemical impedances of a cell. The characteristic impedance curves (Nyquist plots) for the two electrodes are shown in Fig. 7b. In impedance spectroscopy, the high frequency semicircle is attributed to the SEI film and/or contact resistance, while the semicircle in medium frequency region is assigned to the charge–transfer impedance on electrode/electrolyte interface. The inclined line at an approximate 45° angle to the real axis corresponds to the lithium-diffusion process within electrodes [31–33]. It is shown that the diameter of the semicircle in medium frequency region for the nanostructured CoO/Cu electrode is smaller than that of planar electrode, revealing lower charge–transfer impedances, indicating that the charge–transfer process of the nanostructured CoO/Cu electrode has been improved due to the nanostructure of Cu current collectors.

The nanostructured CoO/Cu electrode and planar CoO/Cu electrode were also tested for their rate capability. Fig. 8a compares the discharge capacities of the two electrodes at current rates between 0.3 C and 10 C. Good rate capacity is observed for the nanostructured electrode with capacity retention of 66.5% between 0.3 C and 10 C, which is much higher than that of planar electrode (only about 5%). Even at 10 C (7160 mA g^{-1}), the electrode is capable of delivering stable capacity of 530 mAh g^{-1} (much higher than graphite capacity: 372 mAh g^{-1}). Upon decreasing the rate from 10 C to 0.3 C, nearly 100% of the initial capacity at 0.3 C (about 800 mAh g^{-1}) can be recovered, while the planar electrode can just only recover 42% of the initial capacity. The structural stability of nano-electrode materials during cycling plays a critical role in their cycling performance, which can be confirmed by morphologies of the electrode after cycling. Fig. 8b shows the SEM image of nanostructured CoO/Cu electrode after 50 discharge/charge cycles at various C rates. As observed, the CoO active material layer still sticks on the Cu nanorod surface and no appreciable change in morphology could be noticed, which can explain the excellent power capability and capacity retention of the nanostructured CoO/Cu electrode.

4. Conclusions

Nanostructured hybrid CoO/Cu electrodes were synthesized through electrodeposition and RF-sputtering. When applied as the anode material for lithium-ion batteries, the nanostructured hybrid CoO/Cu electrode delivers a capacity of 970 mAh g^{-1} at a current of 0.3 C after 200 discharge/charge cycles. Even at 10 C (7160 mA g^{-1}), the electrode is capable of delivering stable capacity of 530 mAh g^{-1}. Upon decreasing the rate from 10 C to 0.3 C, nearly 100% of the initial capacity at 0.3 C (about 800 mAh g^{-1}) can be recovered. The electrochemical performance of the nanostructured hybrid CoO/Cu electrode is much better than planar CoO/Cu electrode, which can be attributed to the large accessible surface area and improved electronic/ionic conductivity of the nanostructured electrodes.

Acknowledgments

The authors would like to appreciate the financial support from the 863 Project (No. 2011AA050517), NSFC (No. 51002133) and Innovation Team Project of Zhejiang Province (2009R50005).

References

[1] J.B. Goodenough, Y. Kim, Chem. Mater. 22 (2010) 587–603.
[2] J.M. Tarascon, M. Armand, Nature 414 (2001) 359–367.
[3] P. Poizot, S. Laruelle, S. Grugeon, L. Dupont, J.M. Tarascon, Nature 407 (2000) 496–499.
[4] J. Zhong, X.L. Wang, X.H. Xia, C.D. Gu, J.Y. Xiang, J. Zhang, J.P. Tu, J. Alloys Compd. 509 (2011) 3889–3893.
[5] K.T. Nam, D.W. Kim, P.J. Yoo, C.Y. Chiang, N. Meethong, P.T. Hammond, Y.M. Chiang, A.M. Belcher, Science 312 (2006) 885–888.
[6] N. Du, H. Zhang, B.D. Chen, J.B. Wu, X.Y. Ma, Z.H. Liu, Y.Q. Zhang, D.R. Yang, X.H. Huang, J.P. Tu, Adv. Mater. 19 (2007) 4505–4509.

[7] G.X. Wang, Y. Chen, K. Konstantinov, J. Yao, J.-H. Ahn, H.K. Liu, S.X. Dou, J. Alloys Compd. 340 (2002) L5–L10.
[8] W. Wen, J. Wu, J. Tu, J. Alloys Compd. 513 (2012) 592–596.
[9] Y. Yu, G. Ji, J. Cao, J. Liu, M. Zheng, J. Alloys Compd. 471 (2009) 268–271.
[10] Z. Wu, L. Qin, Q. Pan, J. Alloys Compd. 509 (2011) 9207–9213.
[11] X.H. Xia, J.P. Tu, J.Y. Xiang, X.H. Huang, X.L. Wang, X.B. Zhao, J. Power Sources 195 (2010) 2014–2022.
[12] B. Wang, Y. Wang, J. Park, H. Ahn, G. Wang, J. Alloys Compd. 509 (2011) 7778–7783.
[13] J. Zhu, Y.K. Sharma, Z. Zeng, X. Zhang, M. Srinivasan, S. Mhaisalkar, H. Zhang, H.H. Hng, Q. Yan, J. Phys. Chem. C 115 (2011) 8400–8406.
[14] C. Wang, D. Wang, Q. Wang, L. Wang, Electrochim. Acta 55 (2010) 6420–6425.
[15] Y. Qi, N. Du, H. Zhang, P. Wu, D. Yang, J. Power Sources 196 (2011) 10234–10239.
[16] X. Huang, Y. Yuan, Z. Wang, S. Zhang, F. Zhou, J. Alloys Compd. 509 (2011) 3425–3429.
[17] J. Yang, M. Wang, Y. Zhu, H. Zhao, R. Wang, J. Chen, J. Alloys Compd. 509 (2011) 7657–7661.
[18] P.L. Taberna, S. Mitra, P. Poizot, P. Simon, J.M. Tarascon, Nat. Mater. 5 (2006) 567–573.
[19] A. Finke, P. Poizot, C. Guéry, L.C. Dupont, P.-L. Taberna, P. Simon, J.-M. Tarascon, Electrochem. Solid State Lett. 11 (2008) E5–E9.
[20] L. Bazin, S. Mitra, P.L. Taberna, P. Poizot, M. Gressier, M.J. Menu, A. Barnabé, P. Simon, J.M. Tarascon, J. Power Sources 188 (2009) 578–582.
[21] J. Wang, N. Du, H. Zhang, J. Yu, D. Yang, J. Phys. Chem. C 115 (2011) 23620–23624.
[22] J. Hassoun, S. Panero, P. Simon, P.L. Taberna, B. Scrosati, Adv. Mater. 19 (2007) 1632–1635.
[23] W. Yao, J. Yang, J. Wang, Y. Nuli, J. Electrochem. Soc. 155 (2008) A903–A908.
[24] J. Do, C. Weng, J. Power Sources 159 (2006) 323–327.
[25] X.J. Zhu, Z.P. Guo, P. Zhang, G.D. Du, R. Zeng, Z.X. Chen, S. Li, H.K. Liu, J. Mater. Chem. 19 (2009) 8360–8365.
[26] P. Wu, N. Du, H. Zhang, J. Yu, D. Yang, J. Phys. Chem. C 115 (2011) 3612–3620.
[27] H. Zhang, J. Wu, C. Zhai, X. Ma, N. Du, J. Tu, D. Yang, Nanotechnology 19 (2008) 035711–035715.
[28] J. Zhu, T. Zhu, X. Zhou, Y. Zhang, X.W. Lou, X. Chen, H. Zhang, H.H. Hng, Q. Yan, Nanoscale 3 (2011) 1084–1089.
[29] S. Laruelle, S. Grugeon, P. Poizot, M. Dollé, L. Dupont, J.M. Tarascon, J. Electrochem. Soc. 149 (2002) A627–A634.
[30] J.-S. Do, C.-H. Weng, J. Power Sources 146 (2005) 482–486.
[31] S. Yang, H. Song, X. Chen, Electrochem. Commun. 8 (2006) 137–142.
[32] X.H. Huang, J.P. Tu, C.Q. Zhang, J.Y. Xiang, Electrochem. Commun. 9 (2007) 1180–1184.
[33] T. Zhang, H.P. Zhang, L.C. Yang, B. Wang, Y.P. Wu, T. Takamura, Electrochim. Acta 53 (2008) 5660–5664.